Contract No.:

This manuscript has been authored by Battelle Savannah River Alliance (BSRA), LLC under Contract No. 89303321CEM000080 with the U.S. Department of Energy (DOE) Office of Environmental Management (EM).

Contract No.:

This manuscript has been authored by Battelle Savannah River Alliance (BSRA), LLC under Contract No. 89303321CEM000080 with the U.S. Department of Energy (DOE) Office of Environmental Management (EM).

Highlights

A Framework for Forming Thermoset Polymer Networks during Laser Powder Bed Fusion Additive Manufacturing

Camden A. Chatham, Aaron L. Washington II

- The laser powder bed fusion process has been previously viewed exclusively as a thermoplastic process without regard for activation energy, exothermic heat evolved, or kinetic maxima.
- A conceptual framework is presented for developing thermosetting materials and process parameters for laser powder bed fusion AM. General structure-property-processing relationships are identified for the PBF/L-Thermosets context.
- The conceptual framework is represented mathematically through the "Energy Reaction Ratio (EXR)," which is an adaptation of the well known "Energy Melt Ratio (EMR)."

A Framework for Forming Thermoset Polymer Networks during Laser Powder Bed Fusion Additive Manufacturing

Camden A. Chatham[a], Aaron L. Washington II[b]

[a]*Advanced Engineering Division, Savannah River National Laboratory, Savannah River Site, Aiken, 29808, South Carolina, USA*
[b]*Materials Technology and Energy Division, Savannah River National Laboratory, Savannah River Site, Aiken, 29808, South Carolina, USA*

Abstract

It is commonly reported that the limited availability of material types is a major barrier to widespread adoption for polymer laser powder bed fusion (PBF/L) additive manufacturing (AM). A deeper understanding of the physico-chemical relationships between AM process stimuli and polymer responsive behavior is needed to make data-driven decisions for PBF/L specific material development and formulation. Many researchers have cumulatively built the current state of PBF/L "science-based manufacturing" framework where an initial guess for process parameter values can be determined from measured polymer properties and the first-principles of physics. However, published literature has focused on developing this framework for thermoplastic processing of polymers omitting many specific concerns unique to processing thermosetting materials. The authors consider in the present work the implications of many specific aspects unique to thermosetting polymers during PBF/L manufacturing. These aspects are contextually discussed according to the five sub-functions of PBF/L and are described mathematically where appropriate alongside example data from thermosetting materials commercially available in powder form. This expansion of the prevailing material development framework to include thermosetting polymers paves the way for the unique performance properties offered by that class to be manifest through AM's geometric freedom.

Keywords: laser powder bed fusion, selective laser sintering, thermosetting polymers, covalent network

1. Introduction

Many industries continue to increase their implementation of additive manufacturing (AM) technologies as layerwise fabrication transitions from primarily prototyping applications towards manufacturing of end-use parts. Of the seven technology categories identified by ISO/ASTM 52900 [1], laser powder bed fusion (PBF/L) (also known by the legacy term "Selective Laser Sintering" or SLS) is often championed for end-use production due to its ability to utilize its entire large build volume (e.g., no supports or build plate adhesion requirement) and low anisotropy compared to other AM processes [2, 3]. Additionally, the materials commercially available for PBF/L already include relevant engineering grade polymers, like nylon and PEKK [4]. However, no one family of materials is adequate for every application. Certain applications demand stiff mechanical performance even at elevated temperatures and in the presence of harsh solvents. Traditionally, these performance properties are associated with crosslinked network polymers, which are not currently commercially available for use in PBF/L AM.

The molecular-scale ordering of thermoplastics is based on physical entanglements that are readily lost and reformed through adding energy to the system (e.g., heat), whereas thermosets are covalently bonded networks that are, theoretically, one single polymer chain. Cartoon depictions of these molecular architectures are shown in Figure 1. These two broad categories of molecular architecture influence nearly every performance property. The thermoplastic versus thermoset classification is commonly used to distinguish polymers that are processed solely through physical mechanisms (e.g., solvent swelling, melting, milling, cutting, and pressure-induced flow) from processes that affect a chemical change [5].

The defining characteristic of PBF/L AM as described in ISO/ASTM 52900:2021 is "thermal energy selectively fusing" specific regions of a powder bed in a layerwise manner to fabricate a 3D part [1]. Due to its nature as a thermal process with solid powder-form feedstock, PBF/L is most often used to process thermoplastic polymers. Its use with thermoplastic polymers dates back to the seminal 1979 Housholder patent for "A molding process for forming a three-dimensional article in layers." While the patent claims are written with the more generic terms "solidification" and "fusion," one of the embodiments describes melting plastic powder with no references to

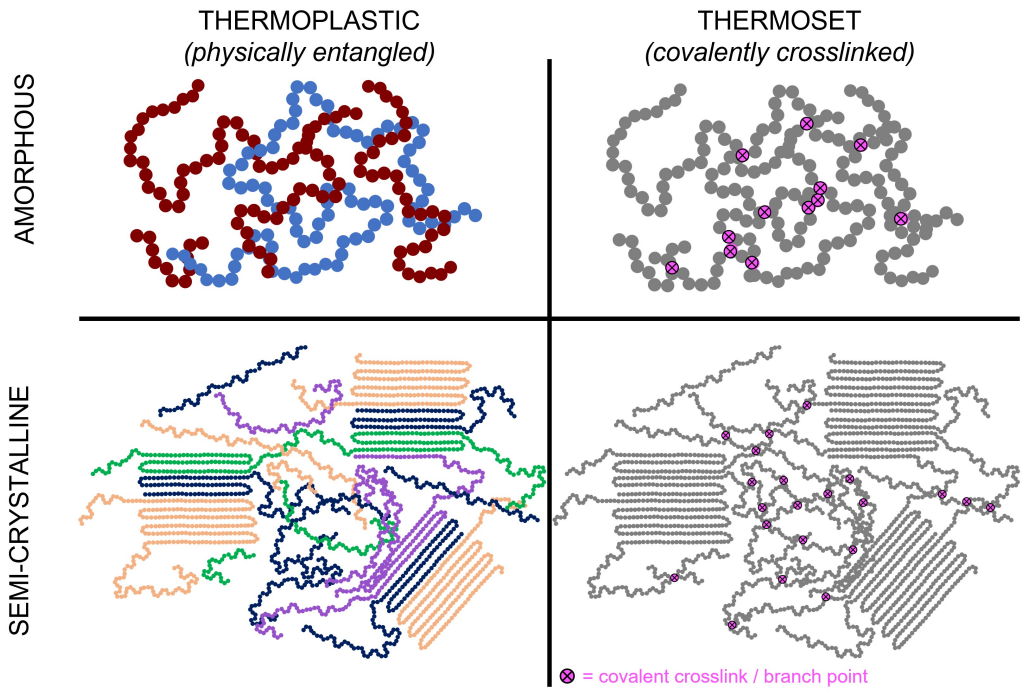

Figure 1: Cartoon depictions of amorphous and semi-crystalline thermoplastics and thermosets. Differing colors in the thermoplastics column indicate individual polymer chains physically interacting with other chains through entanglements and regions of ordered cystals. The unified color of moecules in the thermoset column highlight that a fully-crosslinked polymer is a "single network molecule" where all monomer units are covalently connected to all other monomer units via continuous path. Such differences in molecular architecture have profound implications in polymer properties and processing behavior.

chemical reactions or curing [6]. The same type of language specifying melting with no discussion of chemical reaction dominates papers for subsequent decades [7, 4, 3, 8, 9, 10]. In 2008, Kruth and coauthors mention infiltration of PBF/L printed parts with thermosetting resins as a means to obtain certain performance properties characteristic of network polymers [11]. This idea has been expanded by others [12, 13], but it is not until the conference publication by NASA and the University of Louisville in 2016 [14, 15] and patents by Nguyen and Herzhoff applied for in 2016 then granted in 2020 and 2021 [16, 17] that PBF/L was considered for direct fusion of thermosetting polymers. What little published literature exists for PBF/L of thermosets can be categorized by the point in the manufacturing process relative to the printing step when the network structure is formed: (i) pre-printing, (ii) during printing, or (iii) post-printing.

1.1. Network Formed Pre-printing

Covalent adaptable networks (CAN) are one way to form a network structure pre-print. CANs of poly(dimethyl siloxane) (PDMS) have been demonstrated as printable via PBF/L by Sun, et al. [18]. Additionally, the same researchers have reported PBF/L printing a polyurethane with a dynamic covalent bond based on the Diels-Alder reaction [19].

1.2. Network Formed During Printing

Outside of the patent space, the only published report of forming the network during PBF/L is the authors' prior work [20]. The materials printed were designed to be powder paint coatings and therefore exhibited very brittle properties when formed into freestanding solid structures.

1.3. Network Formed Post-printing

Researchers from NASA report their initial and revised printing efforts for aerospace-grade polyimides [14, 15]. Using their method, an uncrosslinked, near-net shape "green part" is prepared using a DTM Sinterstation PBF/L machine (λ = 10.6 μm) before crosslinking the chain-ends during a 16 h post-print thermal bake. Published work by Hassan, et al. and Campbell, et al. employ similar approaches. Hassan and coauthors use a Sinterit Lisa (λ = 808 nm) to make a bismaleimide green body followed by a 61 h thermal

post-process at various isothermal steps [21]. Campbell and coauthors report printing a two-part epoxide plus amino-sulfone green part with a Sintratec Kit ($\lambda = 455$ nm) prior to crosslinking the chain-ends during an 85 h post-print thermal bake [22].

Outside of Campbell, et al. discussing the importance of slow curing kinetics to avoid shape distortion [22] and the authors' previous work [20], the other articles focus their discussion on heuristic process-printed part performance property relationships. No guidance has been published for selecting process parameter settings based on polymer feedstock properties considering the unique attributes of thermosetting polymers. The authors' present work adapts the conventional guidance for process parameter determination for thermoplastic polymers to include phenomena pertaining to covalent network formation during PBF/L printing. Concepts of energy density, energy melt ratio, energy melt ratio for degradation, and critical coalescence ratio have previously been shown useful for generating initial PBF/L parameter values based on feedstock material properties in the context of PBF/L's five subfunctions [7, 23, 24, 25, 26, 5, 27, 28]. This work discusses thermosetting reactions in the context of the five subfunctions, thus expanding the "science-based manufacturing" framework.

2. Materials and Methods

2.1. Example Thermosetting Powders

One of the most challenging requirements for PBF/L AM is the spherical particle feedstock form. Most polymer PBF/L powders have an average particle diameter between 45-90 μm with a narrow overall distribution between 20-120 μm and are required to be very spherical [2]. Powder paint is one current, commercial application that uses powdered thermosetting polymer precursors; therefore, the following three commercially available off-the-shelf (COTS) powder paints were used in this study: Vulcan Black (TGIC-containing polyester) by Axalta, Oil Black (epoxy-based) by Axalta, and the TD 61 series Anodized Effect (TDA61 TGIC-free polyester) from TIGER Drylac. These materials span three different curing reactions providing multiple crosslink pathways to evaluate in the rapidly cyclic heating environment of PBF/L. These materials have been selected as example materials commercially available in powder form that form a crosslinked network

Table 1: Printing parameters used for each material on a Sintratec Kit.

Material	Chamber Temperature [°C]	Powder Surface Temperature [°C]	Beam Speed [mm s^{-1}]	Layer Height [μm]	Hatch Spacing [μm]	Number of Perimeters	Perimeter Offset [μm]
Vulcan Black (TGIC polyester)	50	70	20, 40, 60	120	80	10	1
TDA61 (TGIC-free polyester)	50	70	20, 40, 60, 150, 235	120	80	10	1
Oil Black (epoxy-based)	50	70	20, 40, 60	120	80	10	1

upon heating. Additionally, data from Satin Black US411N1 (polyurethane-polyester) by ProTech is presented as a negative example of a thermosetting system ill-suited for PBF/L.

2.2. Powder Bed Fusion Additive Manufacturing Machine

All specimens prepared for this work were made using a Sintratec Kit PBF/L additive manufacturing machine (λ = 455 nm). The researchers determined suitable fabrication settings on the Sintratec Kit from previous experimentation to ensure complete and viable parts would be fabricated. These parameters are included in Table 1.

An embedded FLIR X6901SC thermal imaging camera was used to determine the affected maximum temperature and resultant temperature decay profile from the chosen print parameter combination for each material. As all three tested powders are black, they were assumed to have an emissivity of 0.95. Nine regions of interest were defined around a grid of printed cylinders.

2.3. Differential Scanning Calorimetry (DSC)

Samples of powdered feedstock were run on a Mettler Toledo DSC 3+ unit using heating rates of 3, 5, 10, and 20 °C min^{-1}. Test temperature ranges were varied by component material but were conducted to provide at least 25 °C of baseline measurement before and after observed phase transitions and curing reactions. Data analysis to integrate underneath the exothermic curing peaks and generate extent of reaction as functions of time and temperature was performed using the Mettler Toledo STARe software with integral tangential baseline.

Isoconversional analysis was performed on DSC data using Microsoft Excel for linear data fitting. Data were extracted using Excel to the tabular form relating time, temperature, and integrated energy information to percent conversion. These were used to determine activation energy and rate of reaction of each material. Linear fitting to determine activation energy was performed via Kissinger method, shown in Equation 1. In the equation, β is the heating rate, T_p is the absolute temperature at each extent of reaction, E is activation energy at each extent of reaction, and R is the ideal gas constant (8.314 J mol^{-1} K^{-1}). Activation energy was determined at each extent of conversion through the linear fit of Equation 1 of four pairings of β and T_p.

$$ln\left(\frac{\beta}{T_p^2}\right) = \frac{-E}{R}\left(\frac{1}{T_p}\right) \tag{1}$$

Calculations of specific heat capacity were performed according to ASTM E1269-11 [29]. Measurements were conducted on as-received and crosslinked versions of example materials below and above T_g in addition to a sapphire standard reference material.

2.4. Constant-rotation Rheology

The zero-shear viscosity of example COTS materials was determined using a TA Instruments Ares G2 parallel plate rheometer with 25 mm diameter plates. A constant rotation shear-sweep was performed on samples heated just above their melting point (80-95 °C). The Newtonian plateau is extrapolated to estimate the viscosity at "zero shear rate."

3. Results and Discussion

"Science-based manufacturing'" is the idea that relationships drawn from the first-principles of physics and contextualized to a specific manufacturing system or process can be used to generate process parameter values from measured material properties. It is, in a sense, a "feedforward'' attempt to intelligently select the first guess for process parameter values viable for processing a new material never before processed on a particular system. It leverages known material properties for parameter development as an alternative approach to heuristic trial and error. When using this approach, it is often convenient to divide the manufacturing process into its subfunctions to clearly understand the links between material properties and the modes of failure and success at each critical juncture. The five sub-functions of PBF/L are graphically presented in Figure 2 as they are explained by the enumerated claims of the 1979 Housholder patent.

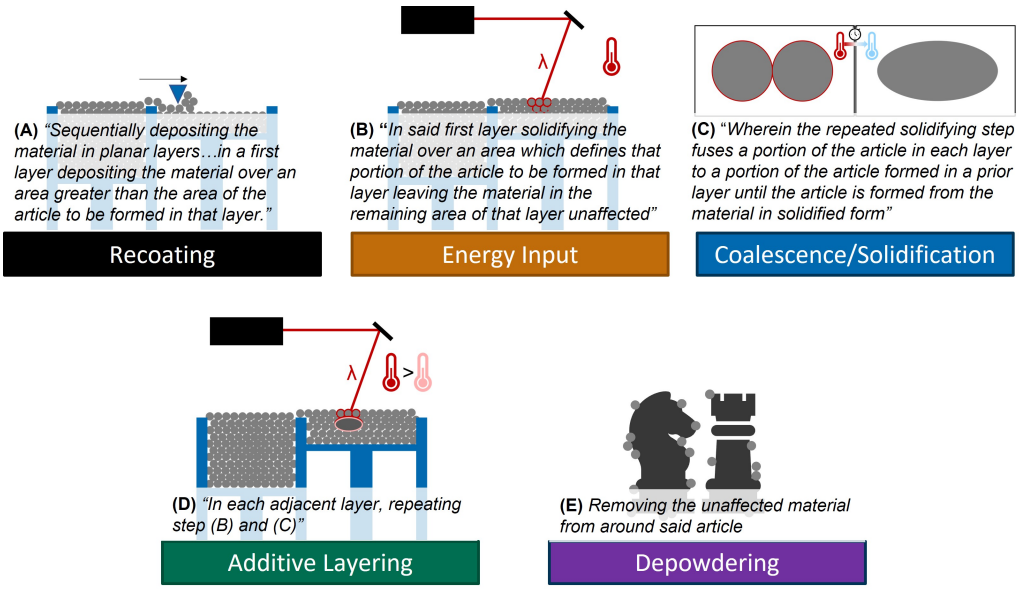

Figure 2: The five sub-functions of laser powder bed fusion. Text quoted from the 1979 Housholder patent claims [6].

There are many differences that exist between thermoset and thermoplastic molecular architecture, however, these differences primarily influence the middle three subfunctions of Energy Input, Coalescence/Solidification, and

Additive Layering. The first subfunction of Recoating and last subfunction of Depowdering are primarily governed by the macroscale properties of the solid powder instead of the optical, thermal, and molten rheological properties that govern the other three. Therefore, this work is scoped to focus primarily on the Energy Input subfunction while briefly discussing Coalescence/Solidification and Additive Layering. The other two subfunctions will not be addressed in this manuscript.

3.1. Subfunction 2: Energy Input

Process parameter value selection for thermoplastic polymers is often centered around the energy melt ratio (EMR) and EMR for degradation first put forward by Starr, et al. [23] and Vasquez, et al. [24] in their work with nylon-12. Chatham, et al. rearranged and expanded the EMR (Equation 2 below; Equation 3 from Reference [7]) to predict minimum and maximum laser power values for their work processing poly(phenylene sulfide) [7].

$$P_{min} = \frac{h \cdot V_b \cdot l}{SC} \cdot [(c_p \cdot (T_m - T_b) + \Delta H_m) \cdot \rho \cdot \Phi] \tag{2}$$

In Equation 2, P_{min} is the minimum power required to achieve full melting of a unit volume of powder material with the standard process parameters of hatch spacing (h), beam speed (V_b), layer height (l), and scan count (SC). The equation describes a material of density ρ, powder packing fraction Φ, and specific heat C_p, being heated from the bed temperature T_b to the polymer's melting temperature T_m. To achieve full melting, the latent heat of melting ΔH_m must also be overcome. To adapt prior work that focused on the purely physical, thermoplastic process to the case of reactive polymers, the following additional topics must be included under the Energy Input subfunction: (i) optical to thermal conversion, (ii) temperature dependent reaction rate, (iii) reaction activation energy, and (iv) the case of a runaway exothermic reaction. As these concerns are specific to encouraging chemical reactions during PBF/L, we will refer to this new, adapted form of the EMR as the Energy Reaction Ratio, "EXR."

3.1.1. Additional Concern 1: Optical to Thermal Conversion

The topic of wavelength-dependence for optical to thermal energy conversion has been largely absent from published PBF/L literature. This may

be explained by the dominance of CO_2 lasers ($\lambda = 10.6$ μm) in PBF/L machines. An article by Tolochko, et al. in 2000 [30] suggested laser wavelength should be a process variable for future investigation, but until the recent advent of PBF/L machines like the Sintratec Kit ($\lambda = 455$ nm), Sintratec S2 ($\lambda = 1060$ nm), Sinterit Lisa ($\lambda = 908$ nm), Formlabs Fuse1 ($\lambda = 1040$ nm), and other such machines CO_2 remained the only relevant laser wavelength for this technology. As seen in the EMR (Equation 2), there is no term representing optical to thermal conversion efficiency thereby assuming that all optical energy supplied by the laser is perfectly converted into heat useful for melting, coalescence, and activating reaction. This is certainly not a valid assumption for all polymers at all wavelengths, as evidenced by the required addition of carbon black for many polymer powders to be printed at shorter wavelengths. Equation 3 includes the new term λ_{eff} to mathematically capture the optical-to-thermal efficiency of a polymer powder at the appropriate laser wavelength.

$$P_{min} = \frac{h \cdot V_b \cdot l}{SC} \cdot \lambda_{eff} \cdot [(c_p \cdot (T_m - T_b) + \Delta H_m) \cdot \rho \cdot \Phi] \tag{3}$$

Many researchers have published on the absorption efficiency of nylon-12 with a CO_2 laser [31, 32, 33, 30]. The chemical reactions present in thermosetting systems have an increased opportunity for wavelength selectivity over the purely physical changes occurring during thermoplastic processing. This idea of wavelength dependency is also well studied for UV curable thermosetting resins in both direct ink write (DIW) [34, 35, 36, 37] and vat photopolymerization (VPP) [38, 39, 40] AM technology families. Outside of the AM context, researchers Lu, et al. report on tuning polymer morphology through a dual-stage polymerization activated and controlled through wavelength dependency [41]. Whether the thermosetting resin relies on an initiator molecule to begin crosslinking or is self-initiating above a certain temperature, wavelength dependency must be quantified to accurately predict process parameter values from material properties.

One method to assess the wavelength dependency of a polymer powder is measuring the affected maximum temperature from a set of process parameters. As seen in Figure 3, there is the expected inverse relationship between scan speed and maximum temperature; however, the specific relationship be-

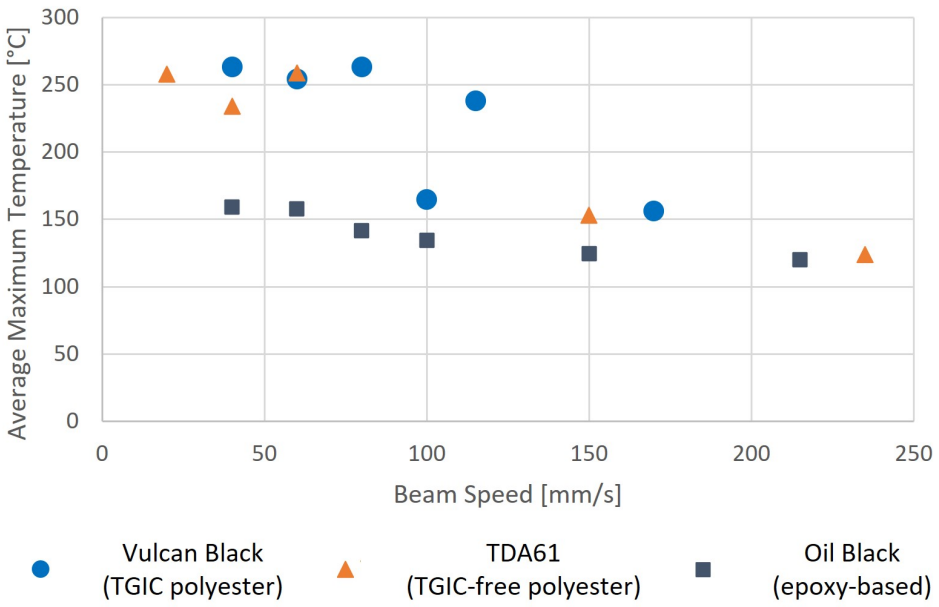

Figure 3: Relationship between average maximum temperature and scan speed for three example materials. Laser wavelength $\lambda = 455nm$.

tween temperature and beam speed is material dependent.

3.1.2. Additional Concern 2: Kinetic Maxima

Many thermoplastic-focused publications define the "PBF/L Processing Window" to fall between the onset of melting when heating and onset of crystallization when cooling as measured in a dynamic DSC experiment [2]. This heuristic method aids in determining the appropriate range for choosing a bed temperature that is hot enough to mitigate out of plane warping but cool enough to maintain spatially selective melting across the powder bed. When transitioning to forming a crosslinked network during printing, there will be no observable crystallization behavior upon cooling in the typical 10 °C min^{-1} DSC experiment as crosslinked networks severely restrict or inhibit crystallization. Although warping and deformation due to crystallization may not be as much of a concern with thermosets, the bed temperature should be set as close to the onset of melting as possible to minimize the difference between curing temperature (T_x) and melting (or glass transition temperature for amorphous precursor materials). The bed temperature must

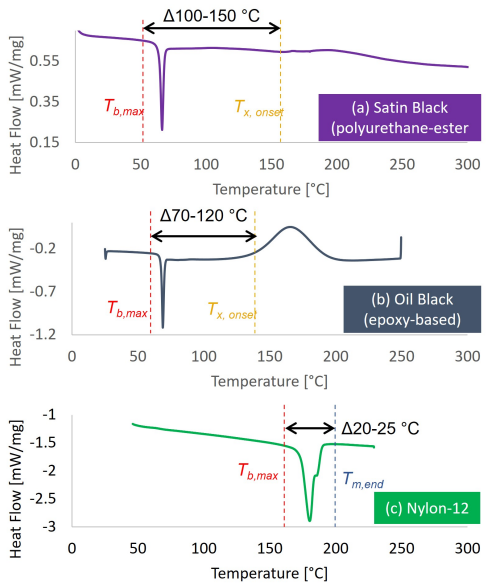

Figure 4: Anotated DSC thermograms of (a) Satin Black US411N1 (polyurethane-polyester), (b) Oil Black (epoxy-based), and (c) Nylon-12 .

remain below the onset of melting to prevent completely melting the entire powder bed, just as with thermoplastics. However, the greater the difference between T_x and T_m the more the material must rely on rapid laser heating to reach cure temperature. Figure 4 depicts DSC thermograms of (a-b) two thermosetting and (c) a thermoplastic resin. The arrows graphically show how much energy must be supplied by the laser to reach the observed onset of crosslinking. The two thermosetting resins have significantly distinct differences between melting and crosslinking at least three-times the typical temperature gap when printing nylon-12. The window between T_m and T_x, onset is significantly smaller for the Oil Black (epoxy-based) (b) than for the Satin Black US411N1 (polyurethane-polyester) (a). If Satin Black US411N1 (polyurethane-polyester) was to be printed, it would not only require more power to cover the temperature gap, but would be further complicated by the greater extremes of temperature cycling affecting the final resulting extent of cure.

Equation 4 changes the target temperature from $T_{m,endset}$, the high-temperature limit of observed melting behavior, to T_x, reflecting mathematically what

Figure 4 shows graphically. When processing semi-crystalline thermoplastic polymers, the goal is to reach a fully molten state to encourage rapid coalescence. This is most reliably achieved by raising the temperature above the equilibrium melting temperature, T_m^0. In this way, the melting phenomenon follows a "higher is better'' paradigm, so long as the temperature remains below degradation. Processing thermosetting polymer systems is more complex. Instead of the T_m^0 threshold, there exists one or more kinetic maxima for the thermosetting system at which the reaction proceeds at the fastest rate. Given the rapid thermal heating and decay cycles characteristic of PBF/L, we hypothesize that a kinetic maximum should be the target temperature affected by laser scanning. Affecting a temperature either below or above a kinetic maximum will limit the extent of reaction. Future work may exploit this phenomenon as a design consideration for targeting specific degrees of crosslinking or else varying the degree of crosslinking throughout the volume of the part. Equation 4 uses the generic T_x as the target temperature for crosslinking. In this work, the authors take $T_x = T_{x,peak}$ to target the maximum possible extent of crosslinking.

$$P_{min} = \frac{h \cdot V_b \cdot l}{SC} \cdot \lambda_{eff} \cdot ([c_p \cdot (T_x - T_b) + \Delta H_m] \cdot \rho \cdot \Phi) \tag{4}$$

Figure 5 depicts the reaction rate as a function of temperature for three example thermosetting polymers. Reaction rate is determined energetically by integrating the area under heat flow vs time data collected at various heating rates in DSC and normalizing the energy released at each timestep to the total energy evolved in the reaction. Each of the example thermosetting systems shown in Figure 5 has a unique cure chemistry, which demonstrates the variety of reaction rate relationships on both temperature and heating rate. Since laser heating is far more rapid than what can be done via conventional DSC instrument, it is expected for any shifts in reaction kinetics with higher heating rates to be even more pronounced in PBF/L conditions.

From the representative *in operando* temperature profile in Figure 5 (d), one observes the rapid decay from maximum temperature achieved during active laser scanning back to the ambient chamber temperature. Even if the scanned area maintained the temperature of maximum rate of reaction for the entire ~6 s of elevated temperature, this would only result in 0.5 % of

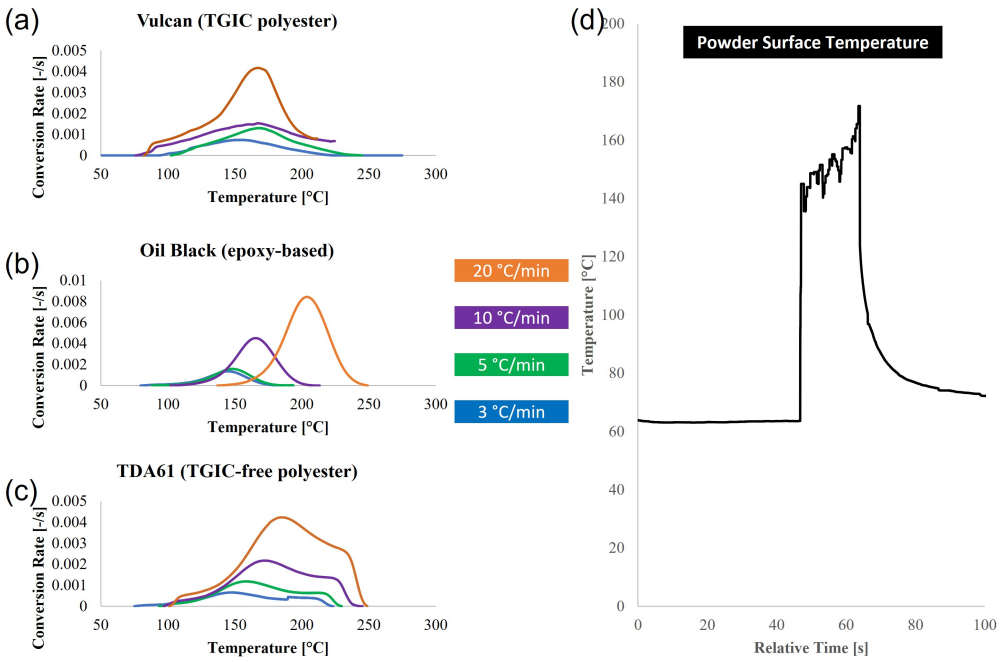

Figure 5: Rate of reaction ($d\alpha/dt$) as a function of temperature at four heating rates for (a) Vulcan Black (TGIC polyester), (b) TDA61 (TGIC-free polyester), and (c) Oil Black (epoxy-based). Curves shown are the average of three replicate trials. Subfigure (d) shows representative temperature versus time data collected via *in situ* thermal camera of the Oil Black (epoxy-based) powder from (c) in a Sintratec Kit (λ = 455 nm) at 40 mm s^{-1} scan speed.

crosslinking. Although complete crosslinking in a single layer is undesired (as will be discussed in greater detail in Section 3.3.2), this number is woefully low. Printing strategies that include multiple scans of the same part area per layer may be one method to increase the time at elevated temperature, but multiple scans per layer is not a commonly editable parameter for commercial PBF/L machines. Alternatively, polymers may be chosen and developed with faster maximum rates of reaction or that continues at lower temperatures after activation. Certainly greater extents of cure are achieved during the VPP process [42, 43]; however, PBF/L's required solid powder form factor may limit what rates are practical to achieve.

3.1.3. Additional Concern 3: Reaction Activation Energy

For the case of materials that undergo a reaction in their melt state, we add the activation energy for the reaction to occur E_{Ax} normalized by molecular weight MW at temperature $T_{x,peak}$, as shown in Equation 5. For the present work, we assume that the onset of crosslinking occurs at a temperature higher than the end of melting (i.e., $T_x > T_m$), otherwise ΔH_m will be zero.

$$P_{min} = \frac{h \cdot V_b \cdot l}{SC} \cdot \lambda_{eff} \cdot \left[\left(c_p \cdot (T_{x,peak} - T_b) + \Delta H_m + \frac{E_{Ax}}{MW} - \Delta H_x \right) \cdot \rho \cdot \Phi \right] \tag{5}$$

Although crosslinking is an exothermic reaction and will be expected to locally raise the temperature, ΔH_x should always be set to zero when computing Equation 5 to determine initial process parameter values. Choosing any other value would artificially decrease the required power predicted. This assumption is valid for the initial layer of a part as the printer must first overcome E_{Ax} before that energy is released; however, ΔH_x will be an important parameter in its own right if modelling the entire process.

Figure 6 depicts the change in activation energy as a function of extent of reaction. Each of the three example materials proceeds via different reaction mechanisms yielding different degrees of variance. Initial activation energy should be chosen when using the EXR to determine initial process

parameter values; however, the energy required to continue the crosslinking reaction changes over time as the reaction progresses. For a material like Vulcan Black (TGIC polyester) (blue circle), the activation energy is greatest for the unreacted state and significantly decreases as the reaction proceeds. This may result in reaching a higher temperature than desired if laser energy is not reduced as the reaction progresses. Conversely, TDA61 (TGIC-free polyester) (orange square) increases the required activation energy with extent of reaction. This may result in a failure to achieve even a moderate extent of cure. The Oil Black (epoxy-based) (gray triangle) has an activation energy with the least variation, only increasing from 24 to 40 kJ mol^{-1} as the reaction progresses. A material with an activation energy relationship like Vulcan Black (TGIC polyester) may be beneficial for PBF/L application as the high initial activation energy serves as a gatekeeper preventing unwanted reaction, but the lower activation energy to continue the reaction at higher extents of conversion may enable crosslinking to occur between layers where the available energy is lower than on the surface.

3.1.4. Additional Concern 4: Runaway Reaction

The so-called "runaway reaction'' occurs when the energy released by one unit volume of material is sufficient to initiate reaction in a neighboring unit volume of material which, in turn, initiates reaction in a neighboring unit volume. The danger and extent of undesired effects for such a case varies anywhere from the slumping shown by Oak Ridge National Lab in their report on using an extrudable thermoset on their Big Area Additive Manufacturing (BAAM) system [44, 45] to the textbook example of an exploding, overheated train car from the reaction of styrene monomer into polystyrene [46]. If this occurs, the inevitable result is continued crosslinking until enough heat can be removed from the nearest neighboring unit volume to not reach T_x and overcome ΔH_m and E_{Ax}. PBF/L systems are intentionally insulated; therefore, heat loss occurs fastest via convection from the top, exposed surface of the unit volume. This concern highlights the important relationship triad of specific heat, thermal conductivity, and heat evolved for PBF/L of thermosetting systems.

The energetic threshold to begin crosslinking during PBF/L comprises the temperature difference between the heated powder bed and the onset temperature where reaction begins to be detectable ($T_{x,onset} - T_b$), specfic

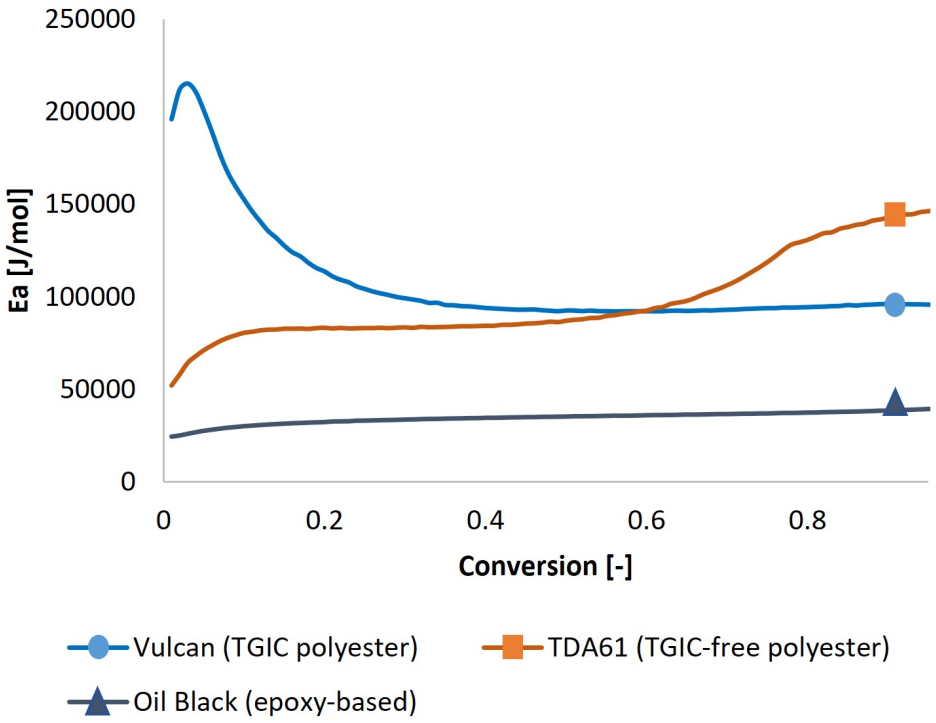

Figure 6: Activation energy as a function of conversion for three example materials. A flat-line relationship would indicate a single-step reaction mechanism for curing, which is not observed for any of the studied materials. Instead, the data suggest complex multi-step reaction pathways for each material that are also different from each other.

heat (c_p), enthalpy of melting (ΔH_m), activation energy ($\frac{EA}{MW}$), and powder geometry factors (Φ and ρ) as arranged in Equation 5 and shown on the right of Equation 6. As the runaway reaction case occurs via conductive heating to a neighboring control volume and not active laser heating, the optical-to-thermal efficiency term λ_{eff} and other laser-specific terms from Equation 5 are not included in Equation 6. The left of Equation 6 mathematically describes the heat evolved from a cylindrical control volume conducting through its surface area by Fourier's Law assuming lumped capacitance. The new variables added are thermal conductivity, κ, the surface area of a cylindrical control volume the size of the laser beam spot, $\pi d\left(d_p + \frac{d}{4}\right)$, to its depth of penetration, d_p, and the layer time in seconds, t_{layer}. The term X represents additional energy supplied by laser heating beyond what was required to melt and affect crosslinking in the intended control volume.

$$X + \left(\pi d\left(d_p + \frac{d}{4}\right)\right) \cdot (\Delta H_x \cdot \rho \cdot d - \kappa \cdot t_{layer}) = \left[c_p\left(T_{x,onset} - T_b\right) + \Delta H_m + \frac{E_{Ax}}{MW}\right] \cdot \rho \cdot \Phi \cdot V \tag{6}$$

Equation 6 simplifies to Equation 7 when a critical volume (V) is chosen to be an anulus of inner diameter equal to the outer diameter of the original control volume, with height of d_p and thickness equal to the average particle diamater, *D50*. Figure S3 in the Supplemental Information illustrates these dimensions.

$$X + \left(d + \frac{d^2}{4d_p}\right) \cdot (\Delta H_x \cdot \rho \cdot d - \kappa \cdot t_{layer}) = \left[c_p\left(T_{x,onset} - T_b\right) + \Delta H_m + \frac{E_{Ax}}{MW}\right] \cdot \rho \cdot \Phi \cdot D50\,(1 + d) \tag{7}$$

The equality in Equations 6 and 7 indicates the critical condition when the energy evolved conducts outside of the unit volume and is able to both raise the temperature of the surrounding single particle of powder and overcome the activation energy to initiate a new reaction; the left side of the equation should be less than the right side to avoid the runaway reaction scenario. A high thermal conductivity will mitigate the build-up of thermal energy that might initiate new reaction. A high specific heat requires more energy to raise the powder temperature, which works cooperatively with activation energy to preserve the selectivity of crosslinking. Conversely, a high curing

enthalpy provides additional energy for unwanted crosslinking. Shown in Figure 4 and tabulated in Table 2, the Satin Black US411N1 (polyurethane-ester) has a lower enthalpy of melting than the Oil Black (epoxy-based). This means there is a lower barrier to melting for the Satin Black US411N1 (polyurethane-ester) than the Oil Black (epoxy-based) and a greater chance of runaway. Conversely, the Oil Black (epoxy-based) also has a larger ΔH_x, meaning more energy is evolved, potentially contributing to unwanted reaction. These properties will need to be carefully considered and balanced for each new material under consideration.

3.2. Subfunction 3: Coalescence and Solidification

Two-particle coalescence behavior in PBF/L has been previously modeled using the Upper-convected Maxwell (UCM) equation [47, 48, 49, 50, 5] as an extension of the generic "viscous sintering of polymers'' mathematical representation by Bellehumeur [51] and originally by Frenkel [52]. While numerical modeling of this process can be quite complex, the scaling relationship is summarized by the Deborah number for coalesce in Equation 8. In Equation 8, λ represents characteristic relaxation time, Γ represents surface energy, η_0 represents zero-shear rate viscosity, and a_0 represents initial particle diameter. The meaning of these symbols are specific to Equation 8.

$$De = \frac{\lambda \Gamma}{\eta_0 a_0} \tag{8}$$

The Deborah number implies that coalescence is encouraged through high relaxation time and surface energy, and opposed by high viscosity and large particle size. Aside from the feedstock-dependent particle size, these properties show temperature dependence in purely thermoplastic processing [9, 53], but also change as a function of network formation [54, 55, 56]. Two additional concerns are considered for the Coalescence/Solidification subfunction in the present work: (i) localized temperature increases from the exothermic process resulting in increased coalescence and part growth and (ii) increased viscosity opposing coalescence resulting from the increased molecular weight/network architecture of a thermosetting system.

3.2.1. Additional Concern 5: Part Growth from Exothermic Reaction

For the case of part growth, the unique concern occurs when heat evolved from the crosslinking reaction (ΔH_x) raises the temperature of a neighboring unit volume to T_m and at least partially overcomes ΔH_m resulting in melting. Equation 9 communicates this concept mathematically, assuming that the solid state of the polymer powder is held together by ordered, crystalline regions. If this is not the case, such as for an amorphous polymer, the definition between fused part and surrounding loose powder is kept by a high viscosity preventing diffusive motion on the length-scale the size of the particle. Note that the reaction specific components of the EXR are omitted from Equation 9 since the concern here is additional coalescence from thermal bleed, which does not involve optical-to-thermal energy conversion and is assumed to occur at a lower temperature than onset of reaction. Exactly raising the temperature to $T_{m,onset}$ will not result in partial melting, but any additional energy would begin the melting process for regions of small crystals. This concept is indicated by the inequality in Equation 9.

$$\Delta H_x > [(C_p \cdot (T_m - T_b)) \cdot \Phi] \tag{9}$$

Depending on whether the neighboring unit volume is inside or outside of the desired geometry, the additional temperature increase may be regarded as beneficial or detrimental. If the neighboring unit volume is outside the desired geometry, the additional melting would be considered undesirable and would decrease the dimensional accuracy of the printed part. If the neighboring unit volume is inside the desired geometry, the additional melting would alter the theoretically predicted P_{min} and P_{max} values, decreasing both proportional to ΔH_x. This is likely to have a trivial effect on actual processing, unless operating at either of the extreme ends of the theoretically predicted processing range or else if one particular unit volume neighbors significantly many scan paths. For example, a designed hole may fuse closed or else two nested parts may fuse together resulting from the additional heat evolved from the crosslinking reaction.

3.2.2. Additional Concern 6: Coalescence Inhibition from Molecular Weight/Architecture Changes

The effect of crosslinking on viscosity is well-documented for many thermosetting polymer systems as it is a primary means of identifying gelation

and extent of reaction. Viscosity often drastically increases even with moderate increases of crosslinking, as exemplified in References [57, 58, 59]. Such behavior manifests as a reduction of powder coalescence rate at high extents of conversion in accordance with the Deborah number scaling relationship. Increased viscosity is the likely cause for effective activation energy increase for the TDA61 (TGIC-free polyester) shown in Figure 6 as it forms a kinetically limiting network morphology. At higher extents of conversion, more energy is required for molecules to diffusively move into available reaction sites.

The effect of crosslink density on surface energy depends on if the reaction alters the hydrophobicity of the surface. If no such change is affected, surface energy is expected to remain constant; however, Zhao and coauthors report changes in surface stress with crosslink density when polymer gels exceed some system-specific critical density [60]. This results from the loss of molecular mobility that comes from crosslinking. The same phenomenon reduces coalescence-relevant relaxation time, thereby opposing particle coalescence.

3.3. Subfunction 4: Additive Layering

Initial investigations of polymer "printability'' focus on the one-layer thick unit volume; however, true printability must consider the effect of subsequent layer formation on the layer of interest (i.e., the effect of layer *n+1* on layer *n*).

3.3.1. Additional Concern 7: Dynamic Material Properties as a Function of Network Formation

In PBF/L, the effect of subsequent layering is predominantly considered as reheating at a given time interval corresponding to average layer time [5, 49, 50]. Material properties are often assumed constant over time at a constant temperature for thermoplastic polymers undergoing purely physical changes. However, as a polymer network is formed, the number, type, and location of present chemical bonds change, which substantially alters the material properties discussed in previous sections. This presents a significant challenge for both process modelling and understanding feedstock-process-structure-property relationships for fabricating thermoset networks during PBF/L. Figure 6 demonstrates this phenomenon for activation energy. By

way of additional example, Table 2 includes values for several material properties included in the EXR framework measured before and after crosslinking. This comparison illustrates the magnitude of change for the selected property values that occurs during crosslinking. The values reported as "(post)" are measured following the manufacturer recommended curing time and temperature schedule and serve as the idealized upper-bound.

Table 2: Selected EXR-relevant material properties for thermosetting systems measured before and after crosslinking. Properties measured by DSC are reported as the average of three trials. Specific heat reported is for the glassy state. Viscosity is measured at 80 °C for the Oil Black (epoxy-based) sample and 95 °C for all other samples.

Material Property:	Vulcan Black (TGIC polyester)	TDA61 (TGIC-free polyester)	Oil Black
T_g [°C] (pre)	66.4 ± 1.6	64.7 ±1.5	65
T_g [°C] (post)	78.4 ± 1.0	65.1 ± 2.7	11
$C_p[Jg^{-1}K^{-1}]$ (pre)	1.39 ±0.35	1.71 ± 0.33	1.5
$C_p[Jg^{-1}K^{-1}]$ (post)	$0.747 \pm 0.731 \cdot 10^{-3}$	$0.688 \pm 11.4 \cdot 10^{-3}$	1.15
$\Delta H_m[Jg^{-1}]$	6.12 ±0.10	8.33 ±0.50	9.
$\Delta H_x[Jg^{-1}]$	26.7 ±3.81	31.0 ±10.6	89
$\eta_0[kPa \cdot s]$	264	95	

3.3.2. Additional Concern 8: Partial Crosslinking

It is not desired to drive the crosslinking reaction to completion within a single layer. Doing so prevents inter-layer covalent crosslinks from forming thereby reducing the printed part to a stack of individually crosslinked thin films with limited mechanical integrity. The ideal method for network formation during PBF/L printing involves complete crosslinking of the "bulk'' polymer chains within one layer while leaving a remnant of surface chains to react with future layers. In order to achieve this secondary, surface crosslinking, the temperature profile must affect a low rate of reaction during lag time between laser scanning events but reheat sub-surface layers to a temperature that overcomes activation energy and drives the reaction forward. This might be achieved through direct reheating during laser scanning if the depth of penetration is greater than the layer height, or else by conductive heating if the volumetric heat generation from the laser beam does not penetrate far into the bed.

These concerns are similar to those of VPP-AM where high crosslink densities result in brittle parts [38]. Prior literature focusing on materials development for VPP centers on creating a working curve from the so-called Jacob's Equation [61]. Although much can be learned by studying VPP methods, the deviation from certain key assumptions will require significant adaption for use in PBF/L. Such deviations include the opaque, solid-state powder used in PBF/L versus the transparent, liquid resin used in VPP. It is known that VPP resins with opaque fillers or emulsified domains scatter light very differently than transparent, homogeneous resins [62, 63]. Additionally, it is common for VPP parts to be subject to a post-cure to further react layers which were only partially cured during active printing [64, 65]. Performing the complete cure in two stages – (i) during shape formation and (ii) following shape formation – encourages covalent bonds to form between layers. Although the premise of the present work aims to form a complete covalent network structure during PBF/L to avoid the additional time and effort observed in prior work [14, 15, 21, 22], such a paradigm may be practically unavoidable for production scenarios.

One helpful diagram summarizing the effects of time and temperature on the cured network is the Time Temperature Transformation (TTT) diagram originally put forward by Enns and Gillham [66]. The "S" shaped diagram describes the extent of cure in terms of glass transition temperature and time to gelation. Complete conversion can only occur when the material is allowed to react for long enough above the glass transition temperature of the final product. Although the maximum temperatures measured in Figure 3 are above the values for T_g *(post)* reported in Table 2, the bed temperature (T_b) used is less than the post-cure T_g for all example materials except TDA61 (TGIC-free polyester). Therefore, the complete reaction does not have the opportunity to occur due to kinetic limitations imposed by vitrification of the growing covalent network. It will be critical to determine whether a set of process parameters affords enough time at temperature to reach gelation before vitirification even if complete conversion does not occur. Future work should include applying the TTT diagram to the cyclical temperature profile typical of PBF/L.

4. Summary and Future Work

Work presented in this manuscript centers on closing the gap for fabricating a covalent network polymer during laser powder bed fusion additive manufacturing processing. The equations used for theoretical determination of process parameter values were expanded from their original forms that only included considerations of thermoplastic polymer processing to include polymer properties unique to thermosetting systems, such as activation energy and the temperature of maximum rate of reaction. Initial process parameter values may now be predicted via the new form of the Energy Melt Ratio (EMR) equation, termed Energy Reaction Ratio (EXR) towards science-based manufacturing. Data were included to showcase the differences in behavior between the most common thermoplastic polymer processed via PBF/L (nylon-12) and commercially available powdered thermosetting systems. A summary of six key differences is presented:

- Laser wavelength dependence is critical for initiating certain reactions.
- The temperature difference between onset of melt (or glass transition) and onset of crosslinking should be minimized.
- Process parameter value selection paradigm shifts from a "minimum threshold to exceed" to "specifically targetting" the temperature of maximum rate of reaction.
- Exothermic reactions may unwantedly heat adjacent volumes of powder resulting in poor geometric fidelity or a runaway reaction.
- Although complete coalescence and complete crosslinking are desired for strong parts, these phenomena oppose each other.
- Polymer response (activation energy, viscosity, surface energy, etc.) to constant manufacturing stimuli changes throughout the print as crosslinking alters molecular architecture.

As with the EMR, the EXR must be evaluated on multiple polymer families to evaluate universality. The case for the EXR was presented with the assumption of using the PBF/L process to form a network polymer from intentionally designed precursors. Another application for the EXR is when

printing "thermosetting thermoplastics," like poly(phenylene sulfide) and polyethylene, which are typically processed under thermoplastic conditions, but can be branched or crosslinked under certain conditions. Chatham, et al. has previously reported this phenomena ocurring with PPS in the PBF/L context [67]. However, thermosetting thermoplastics represent a small fraction of thermosetting polymers, even if they may be the easiest to transition into a PBF/L context.

This work focused on Subfunction 3: Energy Input. Future work should include a more detailed study of the other PBF/L Subfunctions, particularly Subfunction 4: Coalescence/Solidification. It is very likely that the process parameters that are predicted to affect the highest degree of fusion based on conventional thermoplastic-based models will overestimate consolidation for their failure to account for changes brought on by chemical reaction. Future work should consider the balance between particle fusion and degree of crosslinking – particularly crosslinking across particle and layer interfaces. These are competing effects that both generally contribute to overall part strength and stiffness, albeit at different levels of density. Exploiting this effect may open a significant design space, particularly with AM's promise of functionally graded materials.

5. Acknowledgements

The authors thank Supreet Thale of Christopher Williams' Design, Research, and Education for Additive Manufacturing Systems (DREAMS) Lab at Virginia Tech for zero-shear viscosity measurement. This work was produced by Battelle Savannah River Alliance, LLC under contract number 89303321CEM000080 with the U.S. Department of Energy. Publisher acknowledges the U.S. Government license to provide public access under the DOE Public Access Plan (http://energy.gov/downloads/doe-public-access-plan).

References

[1] ASTM/ISO 52900 - additive manufacturing - general principles - terminology (2021).

[2] C. A. Chatham, T. E. Long, C. B. Williams, A review of the process physics and material screening methods for polymer powder bed fusion additive manufacturing, Progress in Polymer Science 93 (2019) 68–95. doi:10.1016/j.progpolymsci.2019.03.003.

[3] R. Goodridge, C. Tuck, R. Hague, Laser sintering of polyamides and other polymers, Progress in Materials Science 57 (2) (2012) 229–267.

[4] A. Das, C. A. Chatham, J. J. Fallon, C. E. Zawaski, E. L. Gilmer, C. B. Williams, M. J. Bortner, Current understanding and challenges in high temperature additive manufacturing of engineering thermoplastic polymers, Additive Manufacturing 34 (2020). doi:10.1016/j.addma.2020.101218.

[5] C. A. Chatham, M. J. Bortner, B. N. Johnson, T. E. Long, C. B. Williams, Predicting mechanical property plateau in laser polymer powder bed fusion additive manufacturing via the critical coalescence ratio, Materials & Design 201 (2021). doi:10.1016/j.matdes.2021.109474.

[6] R. F. Housholder, Molding process, US Patent 4,247,508 (Jan. 27 1981).

[7] C. A. Chatham, T. E. Long, C. B. Williams, Powder bed fusion of poly(phenylene sulfide) at bed temperatures significantly below melting, Additive Manufacturing 28 (2019) 506–516. doi:10.1016/j.addma.2019.05.025.

[8] L. Verbelen, S. Dadbakhsh, M. Van den Eynde, J.-P. Kruth, B. Goderis, P. Van Puyvelde, Characterization of polyamide powders for determination of laser sintering processability, European Polymer Journal 75 (2016) 163–174. doi:https://doi.org/10.1016/j.eurpolymj.2015.12.014.
URL https://www.sciencedirect.com/science/article/pii/S0014305715300938

[9] S. Dupin, Etude fondamentale de la transformation du polyamide 12 par frittage laser: mécanismes physico-chimiques et relations microstructures/propriétés, Ph.D. thesis, INSA de Lyon (2012).

[10] D. Bourell, J. Beaman, H. Marcus, J. Barlow, Solid freeform fabrication an advanced manufacturing approach, in: International Solid Freeform Fabrication Symposium, 1990.

[11] J.-P. Kruth, G. Levy, R. Schindel, T. Craeghs, E. Yasa, Consolidation of polymer powders by selective laser sintering, in: Proceedings of the 3rd International Conference on Polymers and Moulds Innovations, 2008, pp. 15–30.

[12] K. Wudy, T. Budde, Reaction kinetics and curing behavior of epoxies for use in a combined selective laser beam melting process of polymers, Journal of Applied Polymer Science 136 (7) (2018). doi:10.1002/app.46850.

[13] K. Wudy, D. Drummer, Infiltration behavior of thermosets for use in a combined selective laser sintering process of polymers, JOM 71 (3) (2019) 920–927. doi:10.1007/s11837-018-3226-0.
URL https://doi.org/10.1007/s11837-018-3226-0

[14] K. C. Chuang, T. J. Gornet, H. Koerner, Challenges in laser sintering of melt processable thermoset imide resin (2016).

[15] K. C. Chuang, T. J. Gornet, K. Schneidau, H. Koerner, Laser sintering of thermoset polyimide composites (2019).

[16] L.-h. Nguyen, C. Herzhoff, Use of a thermosetting polymeric powder composition, US Patent 10,780,630 (Sep. 22 2020).

[17] L.-h. Nguyen, C. Herzhoff, B. Brüstle, G. Buchinger, Use of a thermosetting polymeric powder composition, US Patent 11,091,660 (Aug. 17 2021).

[18] S. Sun, G. Fei, X. Wang, M. Xie, Q. Guo, D. Fu, Z. Wang, H. Wang, G. Luo, H. Xia, Covalent adaptable networks of polydimethylsiloxane elastomer for selective laser sintering 3D printing, Chemical Engineering Journal 412 (2021) 128675.

[19] S. Sun, X. Gan, Z. Wang, D. Fu, W. Pu, H. Xia, Dynamic healable polyurethane for selective laser sintering, Additive Manufacturing 33 (2020) 101176.

[20] C. A. Chatham, A. L. Washington, A framework with examples for printing thermosetting polymers using laser powder bed fusion additive manufacturing, in: Proceedings of the Solid Freeform Fabrication Symposium, 2022.

[21] M. S. Hassan, K. M. M. Billah, S. E. Hall, S. Sepulveda, J. E. Regis, C. Marquez, S. Cordova, J. Whitaker, T. Robison, J. Keating, E. Shafirovich, Y. Lin, Selective laser sintering of high-temperature thermoset polymer, Journal of Composites Science 6 (2) (2022). doi:10.3390/jcs6020041.

[22] C. G. Campbell, D. J. Astorga, E. Martinez, M. Celina, Selective laser sintering (sls)-printable thermosetting resins via controlled conversion, MRS Communications 11 (2021) 173–178.

[23] T. L. Starr, T. J. Gornet, J. S. Usher, The effect of process conditions on mechanical properties of laser-sintered nylon, Rapid Prototyping Journal (2011).

[24] M. Vasquez, B. Haworth, N. Hopkinson, Optimum sintering region for laser sintered nylon-12, Proceedings of the Institution of Mechanical Engineers, Part B: Journal of Engineering Manufacture 225 (12) (2011) 2240–2248.

[25] M. Vasquez, B. Haworth, N. Hopkinson, Methods for quantifying the stable sintering region in laser sintered polyamide-12, Polymer Engineering & Science 53 (6) (2013) 1230–1240.

[26] G. Vasquez, C. E. Majewski, B. Haworth, N. Hopkinson, A targeted material selection process for polymers in laser sintering, Additive Manufacturing 1 (2014) 127–138.

[27] D. Drummer, D. Rietzel, F. Kühnlein, Development of a characterization approach for the sintering behavior of new thermoplastics for selective laser sintering, Physics Procedia 5 (2010) 533–542.

[28] D. Drummer, K. Wudy, F. Kühnlein, M. Drexler, Polymer blends for selective laser sintering: material and process requirements, Physics Procedia 39 (2012) 509–517.

[29] ASTM E1269: Determining specific heat capacity by differential scanning calorimetry.

[30] N. K. Tolochko, Y. V. Khlopkov, S. E. Mozzharov, M. B. Ignatiev, T. Laoui, V. I. Titov, Absorptance of powder materials suitable for laser sintering, Rapid Prototyping Journal (2000).

[31] M. Schmid, K. Wegener, Additive manufacturing: polymers applicable for laser sintering (ls), Procedia Engineering 149 (2016) 457–464.

[32] T. Laumer, T. Stichel, D. Riedlbauer, P. Amend, J. Mergheim, M. Schmidt, Realization of multi-material polymer parts by simultaneous laser beam melting., Journal of Laser Micro/Nanoengineering 10 (2) (2015).

[33] G. Salmoria, J. Leite, R. Paggi, The microstructural characterization of pa6/pa12 blend specimens fabricated by selective laser sintering, Polymer Testing 28 (7) (2009) 746–751.

[34] J. K. Wilt, D. Gilmer, S. Kim, B. G. Compton, T. Saito, Direct ink writing techniques for in situ gelation and solidification, MRS Communications 11 (2) (2021) 106–121.

[35] A. Dominguez-Alfaro, E. Gabirondo, N. Alegret, C. M. De León-Almazán, R. Hernandez, A. Vallejo-Illarramendi, M. Prato, D. Mecerreyes, 3d printable conducting and biocompatible pedot-graft-pla copolymers by direct ink writing, Macromolecular Rapid Communications 42 (12) (2021) 2100100.

[36] J. W. Kopatz, J. Unangst, A. W. Cook, L. N. Appelhans, Compositional effects on cure kinetics, mechanical properties and printability of dual-cure epoxy/acrylate resins for diw additive manufacturing, Additive Manufacturing 46 (2021) 102159.

[37] J. Bennett, Measuring uv curing parameters of commercial photopolymers used in additive manufacturing, Additive manufacturing 18 (2017) 203–212.

[38] J. M. Sirrine, A. Zlatanic, V. Meenakshisundaram, J. M. Messman, C. B. Williams, P. R. Dvornic, T. E. Long, 3d printing amorphous polysiloxane

terpolymers via vat photopolymerization, Macromolecular Chemistry and Physics 220 (4) (2019) 1800425.

[39] E. M. Wilts, A. Gula, C. Davis, N. Chartrain, C. B. Williams, T. E. Long, Vat photopolymerization of liquid, biodegradable plga-based oligomers as tissue scaffolds, European Polymer Journal 130 (2020) 109693.

[40] N. H. A. Ngadiman, R. Abidin, N. I. S. Murizan, N. M. Yusof, A. Idris, A. Z. A. Kadir, Optimization of materials composition and uv-vis light wavelength towards curing time performance on development of tissue engineering scaffold, Biointerface Res. Appl. Chem 11 (2020) 8740–8750.

[41] H. Lu, P. Huang, T. Wu, C. Chen, J. Shi, M. Xu, L. Qiu, Y. Ding, J. Zhu, Pdlc with controllable microstructure using wavelength-selective two-stage polymerization, Polymer 243 (2022) 124641. doi:https://doi.org/10.1016/j.polymer.2022.124641.
URL https://www.sciencedirect.com/science/article/pii/S0032386122001288

[42] A. M. Clay, J. R. Mitchell, Z. R. Boelter, J. J. La Scala, Superior properties through feedstock development for vat photopolymerization additive manufacturing of high-performance biobased feedstocks, Materials 14 (17) (2021) 4843.

[43] J. Tu, Y. Kashcooli, N. J. Alvarez, G. R. Palmese, A practical framework for predicting conversion profiles in vat photopolymerizations, Additive Manufacturing (2022) 103102.

[44] S. Romberg, C. Hershey, J. Lindahl, W. Carter, B. G. Compton, V. Kunc, Large-scale additive manufacturing of highly exothermic reactive polymer systems, Tech. rep., Oak Ridge National Lab.(ORNL), Oak Ridge, TN (United States) (2019).

[45] S. K. Romberg, A. I. Abir, C. J. Hershey, V. Kunc, B. G. Compton, Structural stability of thin overhanging walls during material extrusion additive manufacturing of thermoset-based ink, Additive Manufacturing 53 (2022) 102677.

[46] P. C. Painter, M. M. Coleman, Essentials of polymer science and engineering, DEStech Publications, Inc, 2008.

[47] C. Balemans, P. Hejmady, R. Cardinaels, P. D. Anderson, Towards unraveling the sintering process of two polystyrene particles by numerical simulations, Korea-Australia Rheology Journal 31 (4) (2019) 285–295.

[48] C. Balemans, S. F. Looijmans, G. Grosso, M. A. Hulsen, P. D. Anderson, Numerical analysis of the crystallization kinetics in sls, Additive Manufacturing 33 (2020) 101126.

[49] A. Mokrane, M. Boutaous, S. Xin, Process of selective laser sintering of polymer powders: Modeling, simulation, and validation, Comptes Rendus Mécanique 346 (11) (2018) 1087–1103.

[50] A. Mokrane, M. Boutaous, S. Xin, Numerical analysis of the heating phase and densification mechanism in polymers selective laser melting process, in: AIP Conference Proceedings, Vol. 1960, AIP Publishing LLC, 2018, p. 140013.

[51] C. T. Bellehumeur, M. Kontopoulou, J. Vlachopoulos, The role of viscoelasticity in polymer sintering, Rheologica acta 37 (3) (1998) 270–278.

[52] J. Frenkel, Viscous flow of crystalline bodies under the action of surface tension, J. phys. 9 (1945) 385.

[53] K. Wudy, D. Drummer, M. Drexler, Characterization of polymer materials and powders for selective laser melting, in: AIP Conference Proceedings, Vol. 1593, American Institute of Physics, 2014, pp. 702–707.

[54] B. Kim, K. Kim, C. Park, C. Ryu, Improvement of wettability and reduction of aging effect by plasma treatment of low-density polyethylene with argon and oxygen mixtures, Journal of adhesion science and technology 16 (5) (2002) 509–521.

[55] D. Schmidt, B. DeKoven, C. Coburn, G. Potter, G. Meyers, D. Fischer, Characterization of a new family of nonwettable, nonstick surfaces, Langmuir 12 (2) (1996) 518–529.

[56] N. Alves, J. L. Gómez Ribelles, J. A. Gómez Tejedor, J. Mano, Viscoelastic behavior of poly (methyl methacrylate) networks with different cross-linking degrees, Macromolecules 37 (10) (2004) 3735–3744.

[57] J. R. Dorgan, D. M. Knauss, H. A. Al-Muallem, T. Huang, D. Vlassopoulos, Melt rheology of dendritically branched polystyrenes, Macromolecules 36 (2) (2003) 380–388.

[58] S. Costanzo, L. F. Scherz, T. Schweizer, M. Kröger, G. Floudas, A. D. Schlüter, D. Vlassopoulos, Rheology and packing of dendronized polymers, Macromolecules 49 (18) (2016) 7054–7068.

[59] A. Van Der Goot, R. Hettema, L. Janssen, The working domain in reactive extrusion. part i: The effect of the polymer melt viscosity, Polymer Engineering & Science 37 (3) (1997) 511–518.

[60] W. Zhao, J. Zhou, H. Hu, C. Xu, Q. Xu, The role of crosslinking density in surface stress and surface energy of soft solids, Soft Matter 18 (3) (2022) 507–513.

[61] P. F. Jacobs, Fundamentals of stereolithography, in: 1992 International Solid Freeform Fabrication Symposium, 1992.

[62] V. Meenakshisundaram, L. D. Sturm, C. B. Williams, Modeling a scanning-mask projection vat photopolymerization system for multiscale additive manufacturing, Journal of Materials Processing Technology 279 (2020) 116546. doi:https://doi.org/10.1016/j.jmatprotec.2019.116546.
URL https://www.sciencedirect.com/science/article/pii/S0924013619305199

[63] S. P. Gentry, J. W. Halloran, Light scattering in absorbing ceramic suspensions: Effect on the width and depth of photopolymerized features, Journal of the European Ceramic Society 35 (6) (2015) 1895–1904. doi:https://doi.org/10.1016/j.jeurceramsoc.2014.12.006.
URL https://www.sciencedirect.com/science/article/pii/S0955221914006633

[64] P. Jindal, M. Juneja, D. Bajaj, F. L. Siena, P. Breedon, Effects of post-curing conditions on mechanical properties of 3d printed clear dental aligners, Rapid Prototyping Journal (2020).

[65] M. Hegde, V. Meenakshisundaram, N. Chartrain, S. Sekhar, D. Tafti, C. B. Williams, T. E. Long, 3d printing all-aromatic polyimides using mask-projection stereolithography: processing the nonprocessable, Advanced Materials 29 (31) (2017) 1701240.

[66] J. B. Enns, J. K. Gillham, Time–temperature–transformation (ttt) cure diagram: Modeling the cure behavior of thermosets, Journal of applied polymer science 28 (8) (1983) 2567–2591.

[67] C. A. Chatham, T. E. Long, C. B. Williams, Process-structure–property relationships following thermo-oxidative exposure of powder bed fusion printed poly(phenylene sulfide), MRS Communications 11 (2) (2021) 179–188. doi:10.1557/s43579-021-00016-0.

[68] A. Patel, A. Maiorana, L. Yue, R. A. Gross, I. Manas-Zloczower, Curing kinetics of biobased epoxies for tailored applications, Macromolecules 49 (15) (2016) 5315–5324.

[69] J. Mijovic, J. Wijaya, Reaction kinetics of epoxy/amine model systems. the effect of electrophilicity of amine molecule, Macromolecules 27 (26) (1994) 7589–7600.

[70] S. C. Leguizamon, N. T. Monk, M. T. Hochrein, E. M. Zapien, A. Yoon, J. C. Foster, L. N. Appelhans, Photoinitiated olefin metathesis and stereolithographic printing of polydicyclopentadiene, Macromolecules 55 (18) (2022) 8273–8282.

[71] C. Kasprzak, J. R. Brown, K. Feller, P. J. Scott, V. Meenakshisundaram, C. Williams, T. Long, Vat photopolymerization of reinforced styrene–butadiene elastomers: A degradable scaffold approach, ACS Applied Materials & Interfaces 14 (16) (2022) 18965–18973.

[72] A. Schmailzl, J. Käsbauer, J. Martan, P. Honnerová, F. Schäfer, M. Fichtl, T. Lehrer, J. Tesař, M. Honner, S. Hierl, Measurement of core temperature through semi-transparent polyamide 6 using scanner-integrated pyrometer in laser welding, International Journal of Heat and Mass Transfer 146 (2020) 118814.

Supplemental Information

Generic Chemical Reactions

Generally speaking, a thermosetting polymer is formed by reacting chemical species with a functionality of greater than two, i.e., at least three potential sites for reaction. A species with only two potential sites for reaction may form a linear chain but has no opportunity to form a covalently bonded network. One example of a molecule with a functionality of three is triglycidyl cyanurate (TGIC) such as used in Vulcan Black (TGIC polyester) in the present work. The chemical structure of TGIC is shown in Figure S 1 with the three oxirane ring functional groups highlighted.

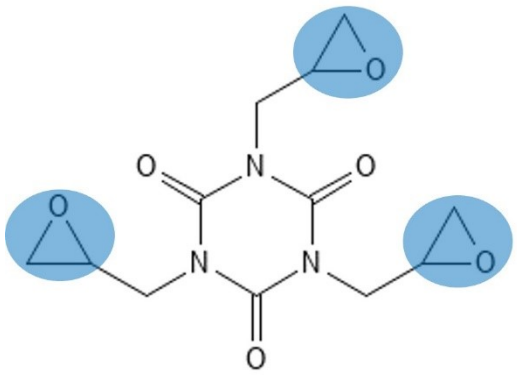

S 1. Triglycidyl isocyanurate (TGIC) chemical structure with three oxirane functional groups highlighted.

Given this basic requirement, reactions generally proceed via the following pathways to achieve a covalently crosslinked network: reaction of monomer species (i) with or without an added initiator species and (ii) with or without laser absorbing additives. Reactions that occur without a dedicated initiator species may be termed "auto-initiating" such as the common epoxy-amine reactions found in References [1] and [2]. The reaction will proceed when reactants ***A*** and ***B*** are in the presence of each other and supplied enough energy to kickoff the reaction. This may also occur with a single species (i.e., ***A*** and ***B*** are chemically the same). In the context of PBF/L, the energy is provided by chamber heating (Δ) and the scanning laser beam (λ) as indicated in Equation S1. Such energetic barriers may be reduced by including a catalyst in the formulation.

$$A + B \xrightarrow{\Delta\lambda} B\{AB\}_n A \qquad \text{Eq. S1}$$

If the reaction will never, or will not practically, autoinitiate, a specific initiator species (***I***) may be included in the formulation. This is common practice in vat photopolymerization AM as indicated by the more detailed References [3, 4, 5]. In this pathway, the energy source breaks a bond within the initiator molecule releasing two radicals (Equation S2) which then react with species A or B to begin propagation reaction (Equation S3).

$$I \xrightarrow{\Delta\lambda} 2I^{-} \quad \text{Eq. S2}$$

$$I^{-} + A + B \rightarrow I\{AB\}_n A \quad \text{Eq. S3}$$

Finally, a laser absorbing species may be included to more efficiently convert the energy supplied at the printer's laser wavelength (λ) into heat (Δ). This is often carbon black. Figure 12a from Schmailzl, et al. shows an increase in carbon black content from 0.3 % w/w to 1.0 % w/w affects approximately a 75 °C temperature increase in the system [6]. Equation S4 shows the laser absorbing species (***L***) as unreactive with the target reactants ***A*** and ***B***; this is the case when including carbon black in a formulation.

$$L + A + B \xrightarrow{\Delta\lambda} B\{AB\}_n A + L \quad \text{Eq. S4}$$

There are a variety of synthetic approaches to achieve a covalent network. Each of them have their unique advantages and drawbacks

Differential Scanning Calorimetry (DSC)

Figure *S 2* shows the full heat-cool-heat behavior for each of the four example thermosetting systems. First heats are designated by "H1," second heats are designated by "H2," and the cooling pass is designated by "C" appended onto the material's trade name.

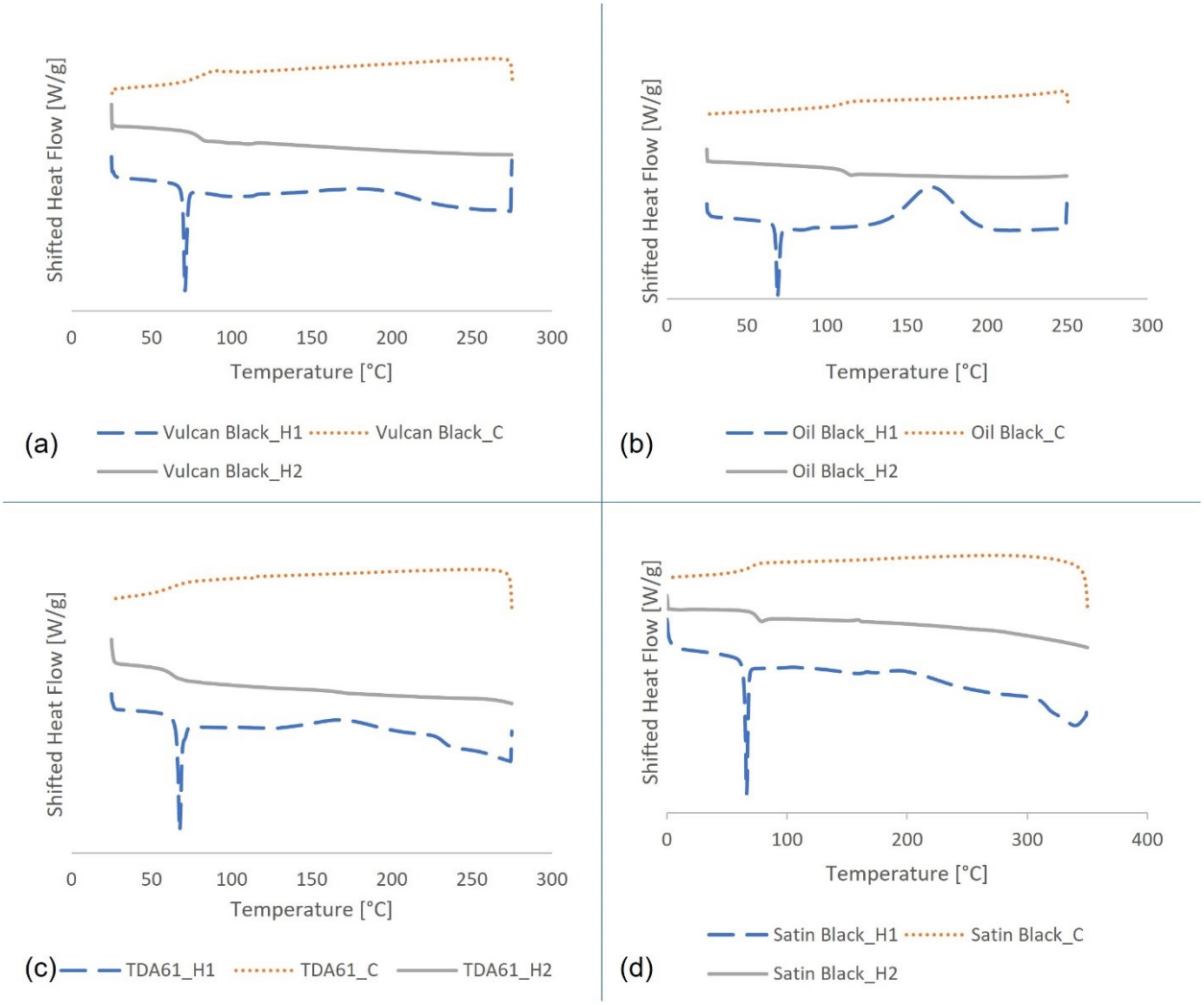

S 2. DSC thermograms for (a) Vulcan Black (TGIC Polyester), (b) Oil Black (epoxy based), (c) TDA61 (TGIC-free polyester), and (d) Satin Black US411N1 (polyurethane-ester). Exotherm plotted up.

Depiction of Heat Transfer in Powder Bed

Figure *S 3* is a cartoon depiction of heat transfer in the powder bed. It corresponds with Equations 6 and 7 from the main paper, reproduced below as Equations S5 and S6 for ease of reference.

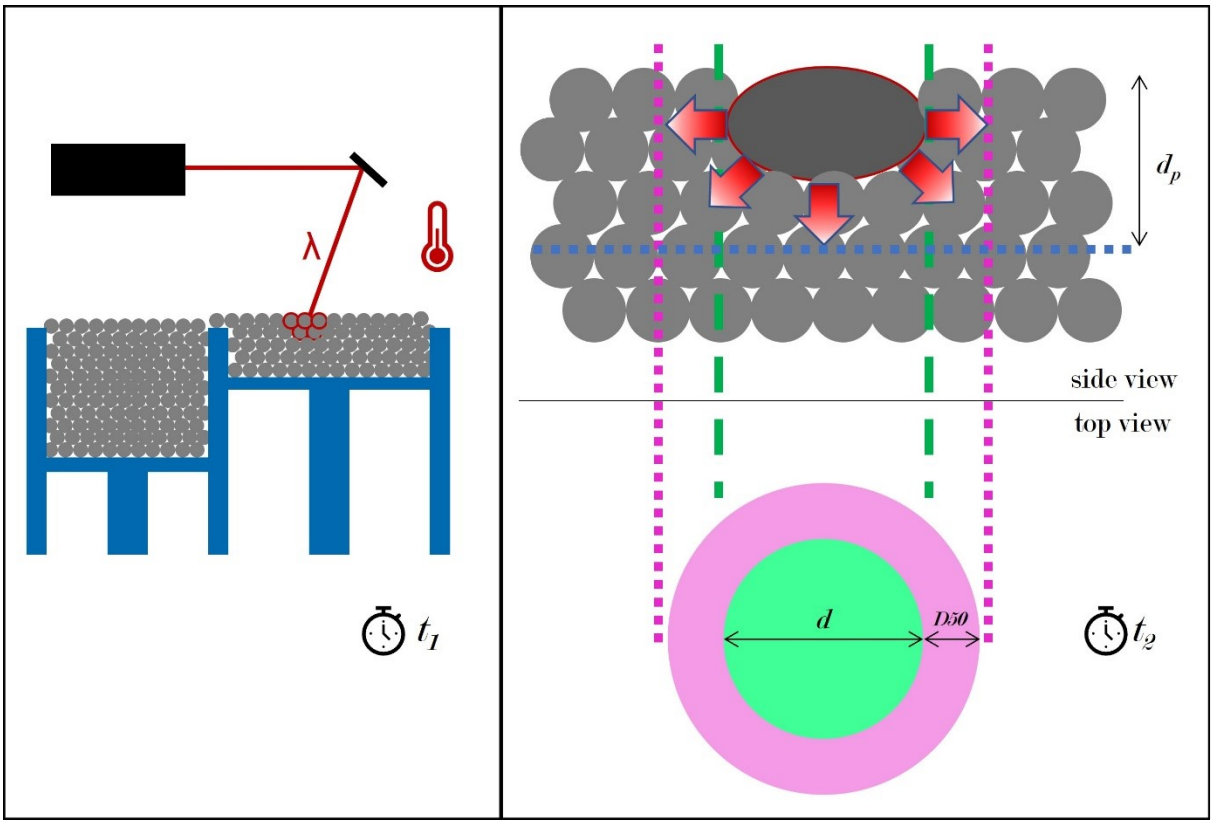

S 3. Cartoon depiction of conductive heat flow out of control body during PBF/L described mathematically in Equations 6 (S5) and 7 (S6).

$$X + \left(\pi d\left(d_p + \frac{d}{4}\right)\right) \cdot \left(\Delta H_x \cdot \rho \cdot d - \kappa \cdot t_{layer}\right) = \left[c_p\left(T_{x,onset} - T_b\right) + \Delta H_m + \frac{E_{Ax}}{MW}\right] \cdot \rho \cdot \Phi \cdot V \quad \text{Eq. S5}$$

$$X + \left(d + \frac{d^2}{4d_p}\right) \cdot \left(\Delta H_x \cdot \rho \cdot d - \kappa \cdot t_{layer}\right) = \left[c_p\left(T_{x,onset} - T_b\right) + \Delta H_m + \frac{E_{Ax}}{MW}\right] \cdot \rho \cdot \Phi \cdot D50(1 + d) \quad \text{Eq. S6}$$

References

[1] A. Patel, A. Maiorana, L. Yue, R. A. Gross and Manas-Zloczower, "Curing kinetics of biobased epoxies for tailored applications," *Macromolecules,* vol. 49, no. 15, pp. 5315-5324, 2016.

[2] J. Mijovic and J. Wijaya, "Reaction kinetics of epoxy/amine model systems: the effect of electrophilicity of amine molecule," *Macromolecules,* vol. 27, no. 26, pp. 7589-7600, 1994.

[3] S. Leguizamon, N. Monk, M. Hochrein, E. Zapien, A. Yoon, J. Foster and L. N. Appelhans, "Photoinitiated olefin metathesis and stereolithographic printing of polydicyclopentadiene," *Macromolecules,* vol. 55, no. 18, pp. 8273-8282, 2022.

[4] C. Kasprzak, J. Brown, K. Feller, P. Scott, V. Meenakshisundaram, C. Williams and T. Long, "Vat photopolymerization of reinforced styrene-butadiene elastomers: A degradable scaffold approach," *ACS Applied Materials and Interfaces,* vol. 14, no. 16, pp. 18965-18973, 2022.

[5] J. Sirrine, A. Zlatanic, V. Meenakshisundaram, J. Messman, C. Williams, P. Dvornic and T. Long, "3D printing amorphous polysiloxane terpolymers via vat photopolymerization," *Macromolecular Chemistry and Physics,* vol. 220, no. 4, p. 1800425, 2019.

[6] A. Schmailzl, J. Kasbauer, J. Martan, P. Honnerova, F. Schafer, M. Fichtl, T. Lehrer, J. Tesar, M. Honner and S. Hierl, "Measurement of core temperature through semi-transparent polyamide 6 using scanner-integrated pyrometer in laser welding," *International Journal of Heat and Mass Transfer,* vol. 146, p. 118814, 2020.